Acta Biomaterialia 101 (2020) 285–292

Contents lists available at ScienceDirect

Acta Biomaterialia

journal homepage: www.elsevier.com/locate/actbio

Full length article

In vitro evaluation of Pt-coated electrospun nanofibers for endovascular coil embolization

Min-Woo Kim[a,1], Seongpil An[b,1], Hyunjun Seok[a], Hyunchul Jung[c], Dong-Hyuk Park[d,*], Alexander L. Yarin[b,*], Sam S. Yoon[a,*]

[a] School of Mechanical Engineering, Korea University, Seoul 02841, Republic of Korea
[b] Department of Mechanical and Industrial Engineering, University of Illinois at Chicago, 842W. Taylor Street, Chicago, IL 60607-7022, USA
[c] E-eung, 1009 Medical Device Complex Center, 200 Gieopdosi-ro Jijeong-myoen, Wonju-si, Gangwon-do, Republic of Korea
[d] Department of Neurosurgery, Korea University Medical Center, Korea University College of Medicine, Seoul, Republic of Korea

ARTICLE INFO

Article history:
Received 13 June 2019
Revised 4 October 2019
Accepted 8 October 2019
Available online 11 October 2019

Keywords:
Endovascular coil embolization
Aneurysm
Electrospinning
Platinum nanofiber
Permeability

ABSTRACT

Recently, endovascular coil embolization has been introduced to treat intracranial aneurysms because it has lower morbidity and mortality than surgical clipping. The endovascular coils prevent the extravasation of blood by decreasing the permeability of an aneurysm flow governed by Darcy's law. Here, we developed and explored Pt-coated micro-ropes for potential use as endovascular coils. Electrospinning with subsequent electroplating were employed to fabricate Pt-coated nanofibers, which were tightly twisted to form micro-ropes. The compatibility of Pt micro-ropes with commercial delivery catheters was verified and their performance was experimentally explored in an in vitro experimental model. The developed Pt-coated micro-ropes demonstrated feasibility as efficient and low-cost endovascular coils.

Statement of Significance

The use of Platinum (Pt)-coated polymer nanofibers to prevent blood extravasation has been demonstrated. These Pt nanofibers were installed within a microfluidic channel, and the resulting reduced permeability was evaluated using a fluid similar to blood. Based on the obtained results, these newly developed nanofibers are expected to decrease the operation cost for aneurysmal subarachnoid hemorrhage (SAH), owing their reduced size and low material cost. Overall, the use of this new material should reduce the operational risk associated with the multiple steps required to place the Pt coils at the SAH site. The compatibility of Pt micro-ropes with commercial delivery catheters was verified and their performance was experimentally explored in an in vitro experimental model. The developed Pt-coated micro-ropes demonstrated feasibility as efficient and low-cost endovascular coils.

1. Introduction

Intracranial aneurysms are pathological dilatations of intracranial arteries characterized by disorganization and disruption of the arterial wall layer. This vulnerable wall is prone to rupture, which causes subarachnoid hemorrhage (SAH). The mortality of aneurysmal SAH is approximately 30%–40%; 50% of survivors suffer various resulting disabilities despite modern neurosurgical treatments [1]. Intracranial aneurysms are currently treated by blocking cerebral circulation into the aneurysm sac via either endovascular coil embolization or microsurgical clipping of the aneurysm neck. Recently, endovascular embolization has become widely accepted as a treatment strategy that is preferred for both ruptured and un-ruptured intracranial aneurysms because it reveals lower periprocedural morbidity and mortality than surgical clipping [2,3]. However, endovascular coil embolization has higher rates of incomplete aneurysm occlusion and aneurysm recurrence after complete occlusion when compared to surgical clipping [3]. Previous studies have reported that the aneurysm recurrence rate after endovascular treatment is between 4.7% and 33% [4–6]. The risk of re-bleeding with endovascular coiling, which ranges from 0.4% to 7.9%, is also somewhat higher than that with microsurgical clipping [3–5].

Because previous studies have shown inverse correlations between the packing density and the recanalization rate of

* Corresponding authors.
E-mail addresses: doctorns@korea.ac.kr (D.-H. Park), ayarin@uic.edu (A.L. Yarin), skyoon@korea.ac.kr (S.S. Yoon).
[1] These authors have equally contributed.

https://doi.org/10.1016/j.actbio.2019.10.015
1742-7061/

Table 1
Experimental conditions for electrospinning and electroplating.

Process	Parameter	Value
Electrospinning	Applied DC voltage [kV]	6
	Flow rate [μl/h]	280
	Needle-to-collector distance [cm]	13
	Electrospinning time [s]	60
Electroplating	Applied DC voltage [kV]	5
	Anode-to-cathode distance [cm]	3
	Electroplating time [min]	5

occlusions, coil packing density is widely considered one of the key factors determining the durability of endovascular embolization [7]. To improve the packing density and thus reduce the recurrence rate of endovascular aneurysm coiling, various modifications of bare Pt coils have been suggested and developed. Covering Pt coils with polymers such as poly(glycolic acid) or poly(lactic acid), which may augment the inflammatory reaction around the neck of the aneurysm, has failed to demonstrate significant differences in comparison with bare Pt coils [8,9]. Hydrogel-coated coils have also been developed, following the rationale of hydrogel expansion upon contact with blood, resulting in an increased packing density [10]. Although first-generation hydrogel coils have reduced the high recurrence rates associated with endovascular coiling, they entail problems of coil stiffness and time restriction for coil deployment [11]. Currently, second-generation hydrogel coils, which are softer and slower to expand, have been developed and tested in endovascular embolization not only to address the aforementioned issues, but also to evaluate and decrease the insertion resistance that is caused by a frictional force between a micro-catheter and inner Pt coils [12–16].

In our previous study, Pt-coated nanofibers were developed and their potential use as endovascular coils was explored in a model hemodynamic setting [17]. The Pt-coated nanofibers fabricated using electrospinning followed by electroplating demonstrated a higher packing density compared to that of the existing Pt coils. Thus, it is expected that they are able to reduce the risk associated with surgical procedures for deploying Pt coils in the aneurysm sac [18]. In this study, we also developed an analytical model of the hemodynamics of coiled aneurysms, which enabled the explanation and quantification of permeability changes resulting from aneurysm coiling in order to further characterize the feasibility of Pt-coated nanofibers. An in vitro experimental model is prepared based on the actual structure of an aneurysm in the present study, and the packing performance of Pt-coated nanofibers is experimentally evaluated in this model. In addition, the compatibility of the Pt-coated nanofibers with commercial delivery catheters is demonstrated through in vitro experiments.

2. Experimental section

2.1. Pt-coated nanofibers

The fabrication process of the Pt-coated micro-ropes is illustrated in Fig. 1a. The details of the fabrication process were described in our previous studies [17,18]. In brief, Pt-coated nanofibers were prepared through two subsequent steps of electrospinning and electroplating. The electrospinning solution of 8 wt% polyacrylonitrile (PAN) was prepared by dissolving PAN (M_w = 150 kDa, Sigma-Aldrich) in *N,N*-dimethylformamide (DMF, 99.8%, Sigma-Aldrich) and stirring for 24 h at room temperature. The electroplating solution was prepared by diluting 80 mL of the Pt HT concentrate (Pt 50 g/L, HanTech PMC) with 4200 mL of deionized (DI) water and stirring for 24 h at room temperature.

Detailed experimental conditions for electrospinning and electroplating are listed in Table 1. The electrospun PAN nanofibers are deposited onto a Cu frame and then electroplated while suspended on the Cu frame (cf. Fig. 1a). It should be emphasized that, before electroplating, the electrospun PAN nanofibers were sputtered with Pt for a few seconds (MSP-1S Vacuum Device Inc.) to impart some conductivity to the non-conductive polymer nanofibers. After electroplating, the resulting Pt-coated nanofiber mats were tightly twisted to form textured Pt-coated micro-ropes (cf. Fig. 1a).

2.2. In vitro experimental model

It should be emphasized that the in vitro model in the present study is designed based on the actual structure of an aneurysm (cf. Fig. 1b and c), which facilitates a more accurate evaluation of the permeability of the bladder in the model compared to that achieved in our previous study [17]. The model is built using transparent acrylic material (Fig. 1c), allowing for easy identification of fluid flow in the model. The complex curved channels and bladder in the model are schematically shown in Fig. 1e in order to calculate the permeabilities to fluid using Darcy's law and the Poiseuille equation (cf. Section 3.3). The distance from the inlet to the bladder is 12.5 cm (see L_1 in Fig. 1e). The distances from the bladder to outlets 1 and 2 are 3 and 6.5 cm, respectively (l_1 and L_2 in Fig. 1e). The diameters of the spherical bladder and the channel inside the model are 30 and 10 mm, respectively (Fig. 1e). The flow rate of the injected fluid is 1 mL·min^{-1}. The injection lasts for 10 min. The blocking effect of the Pt–coated micro-ropes in the bladder was explored by varying the number of inserted micro-ropes (N) from $N=0$ to $N=40$. The corresponding permeabilities of the blockages are obtained by averaging the results of five experiments with each number of micro-ropes.

The fluid used in experiments was 5 wt% polyvinyl alcohol [PVA-1500, practical grade, $(C_2H_4O)_n$, Duksan Pure Chemicals Co. Ltd.] dissolved in DI water, which has a viscosity similar to that of blood (~3 cP). The fluid was dyed with Rhodamine-B for visualization purposes. In addition, unlike the actual structure of an aneurysm, outlet 1 is adjunctively installed in the in vitro model in order to evaluate permeability of the bladder as it is filled by the Pt micro-ropes (cf. Fig. 1c). As the bladder is filled with the micro-ropes, the flow rate of fluid passing into the bladder gradually became smaller, ultimately approaching zero.

Fig. 1d illustrates the endovascular coil embolization using multiple Pt-coated micro-ropes and delivery catheters, where the aneurysmal sac is filled by the micro-ropes, thus preventing blood flow into the aneurysmal sac. First, in order to secure a passage to the aneurysmal sac along the blood vessel, the hollow guide catheter is inserted into the blood vessel and located near the aneurysmal sac (see the second step in Fig. 1d). Then, the micro-catheter is inserted in the core of the guide catheter and delivered to the end of the guide catheter (see the third step in Fig. 1d). Finally, the micro-ropes are consecutively delivered to the aneurysmal sac, gradually filling the aneurysmal cavity (see the fourth step in Fig. 1d).

2.3. Characterization

The morphologies of the nanofibers and textured micro-ropes were examined by high-resolution scanning electron microscopy equipped with energy-dispersive X-ray spectroscopy (HR-SEM/EDX, XL30 SFEG, Phillips Co., Holland) at 15 kV. X-ray diffraction (XRD, Rigaku, Japan, D/max-2500) was performed with Cu Kα radiation over the 2θ range 20°–80° to identify the crystallinities of the PAN and Pt-coated nanofibers. X-ray photoelectron spectroscopy (XPS, Theta Probe Base System, Thermo Fisher Scientific Co.) was also conducted to identify the compositions of the PAN and Pt-coated nanofibers. The cross-sectional and corresponding elemental mapping images of the Pt-coated nanofibers were obtained by

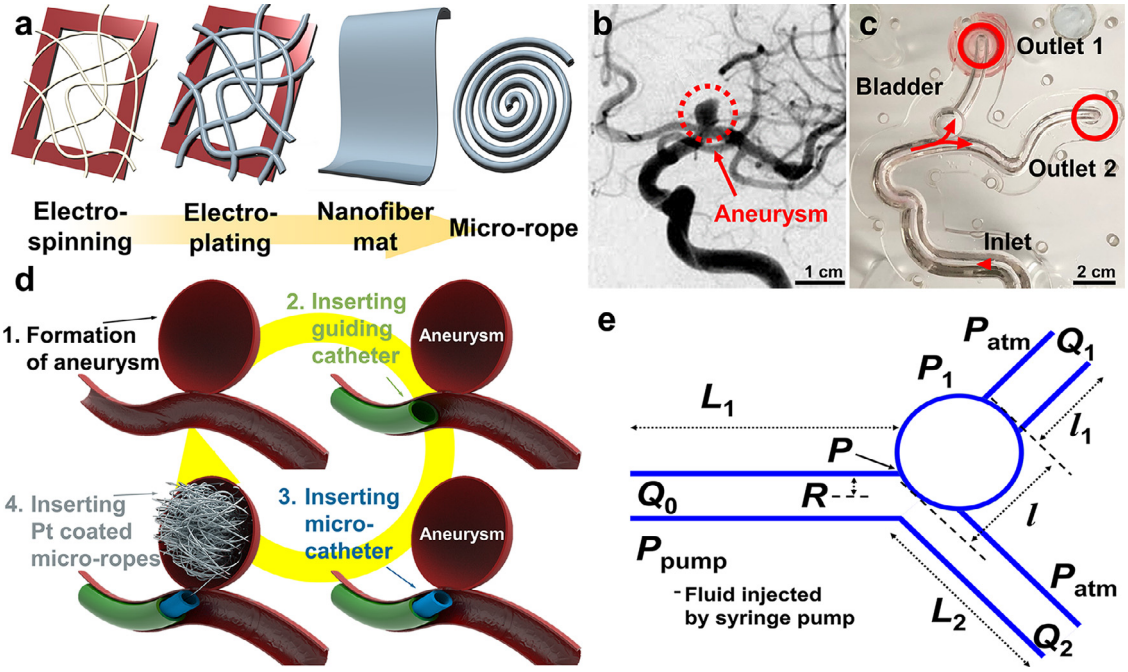

Fig. 1. (a) Fabrication process of the Pt-coated micro-ropes. (b) Angiographic X-ray image of cerebral aneurysm of a patient, and (c) photograph of the in vitro experimental model based on the cerebral aneurysm shown in panel (b). (d) Illustration of the endovascular coil embolization using the Pt-coated micro-ropes and catheters. (e) Schematic of flow in the channels of the in vitro model for permeability calculations.

transmission electron microscopy (TEM, Tecnai G2 F30ST, FEI Company); a focused ion beam (FIB, Quanta 2003D microscope, FEI Company) was used to prepare the specimens for TEM analysis.

3. Results and discussion

3.1. Pt-coated nanofibers and nano-textured Pt-coated micro-ropes

Scanning electron microscopy (SEM) images of the electrospun PAN and Pt-coated nanofibers are shown in Fig. 2. Fig. 2a and b shows the SEM images of individual nanofibers of the pristine PAN and Pt-coated specimens, while Fig. 2c and d shows the corresponding micro-ropes formed from the PAN and Pt-coated nanofibers, respectively. The cross-sectional diameter of the pristine PAN nanofiber is ~320 nm (Fig. 2a) and that of the Pt-coated nanofiber is ~500 nm (Fig. 2b). It should be emphasized that both the PAN and Pt-coated nanofiber mats are twisted into cylindrical micro-ropes, which are elaborately manipulated to have diameters equal to that of a commercial Pt coil (Fig. 2c and d) [17]. As a result, the diameters of both micro-ropes are approximately 250 μm; the length of each micro-rope is 10 cm.

To explore the permeability changes with variation in the diameter of the Pt-coated nanofibers, Pt-coated nanofibers of different diameters are fabricated by varying the electroplating times from 5, 10, to 20 min (Fig. 2e–g). This yields Pt-coated fibers with diameters of 0.50 ± 0.08, 0.75 ± 0.11, and 1.00 ± 0.13 μm, respectively. However, it should be emphasized that the diameters of the micro-ropes formed from the Pt-coated nanofibers of different diameters remain equal to 250 μm. This is achieved by using different numbers of Pt-coated nanofiber mats to form the micro-ropes: 36, 16, and 10 nanofiber mats with nanofiber diameters of 0.50, 0.75, and 1.00 μm, respectively, are used to fabricate each micro-rope. The size of each nanofiber mat is 3 cm × 4 cm.

To better characterize the cross-sectional structures of individual Pt-coated nanofibers, TEM is performed as shown in Fig. 3, where the specimen is prepared by using a FIB milling technique (cf. Section 2.3). The cross-sectional TEM images of Pt-coated

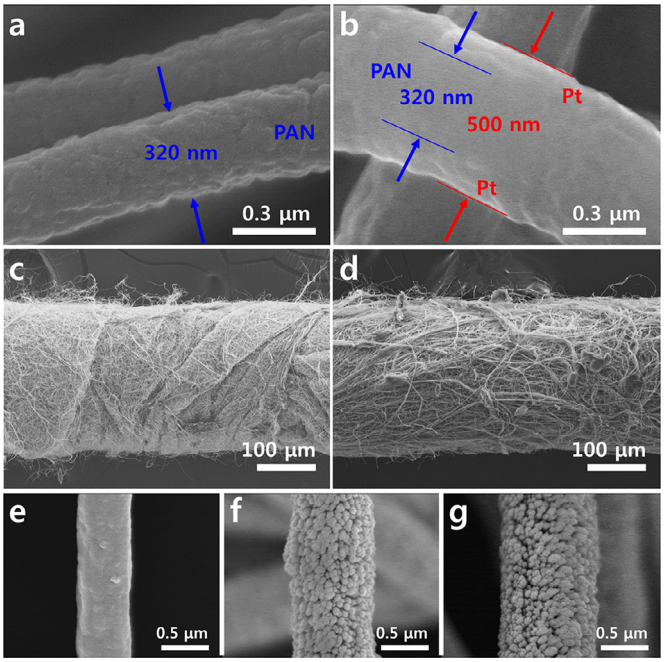

Fig. 2. SEM images of (a) the electrospun PAN nanofibers, (b) the Pt-coated nanofibers, (c) the twisted PAN micro-rope, and (d) the twisted Pt-coated micro-rope. SEM images of the Pt-coated nanofibers with different electroplating times of (e) 5, (f) 10, and (g) 20 min.

nanofibers in Fig. 3a and b clearly show the core-shell structures of the nanofibers, where the PAN core diameter and the Pt shell thickness are 320 and 90 nm, respectively. These results are consistent with those obtained from the SEM images in Fig. 2a and b. It should be emphasized that, not only the probability of the core being exposed to in vivo is very low due to the Pt shell, but also the PAN core can be replaced by biocompatible polymers such as

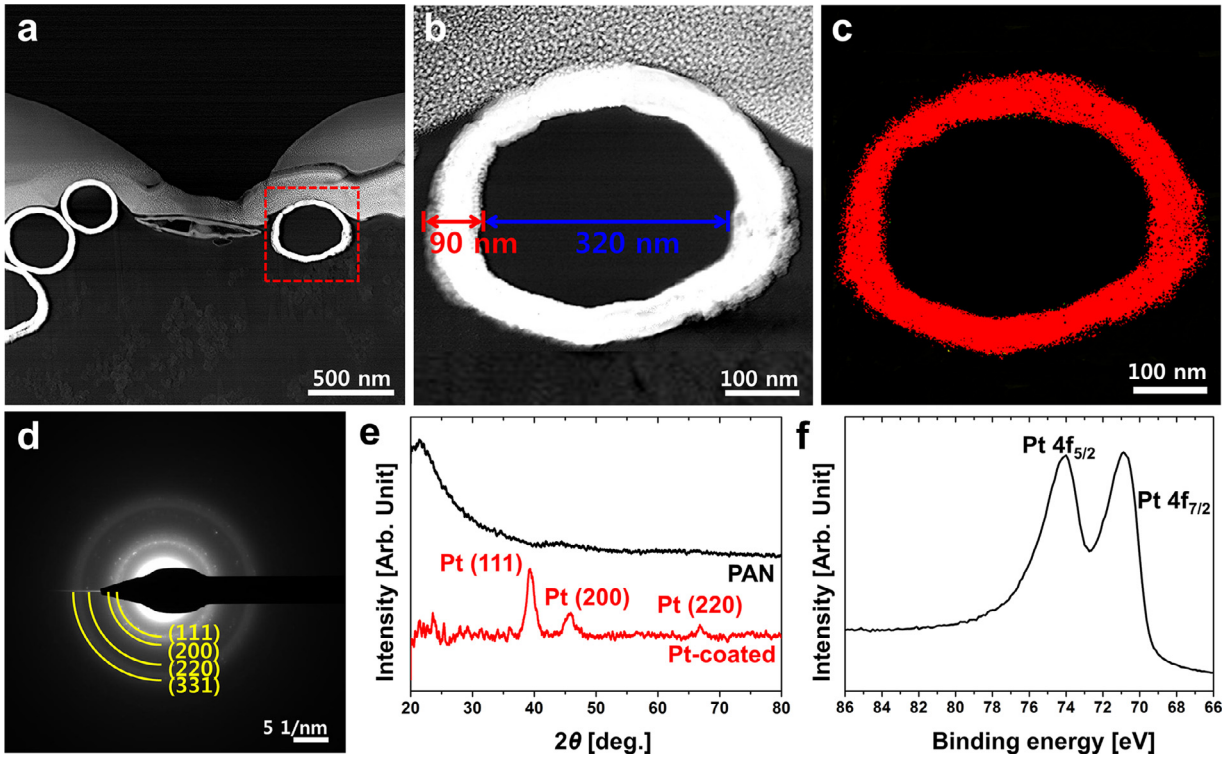

Fig. 3. (a, b) Cross-sectional TEM images of Pt-coated nanofibers. (c) An elemental mapping image of the corresponding Pt-coated nanofiber (where red color indicates Pt element), and (d) the corresponding selected-area electron diffraction (SAED) pattern. (e) XRD patterns of electrospun PAN nanofibers and Pt-coated nanofibers. (f) High-resolution XPS spectrum of Pt 4*f* energy level. (For interpretation of the references to color in this figure legend, the reader is referred to the web version of this article.)

polycaprolactone [17]. In addition, the recent studies demonstrated that PAN can be biodegradable through synthesis with Pectin [19] and sodium silicate [20]. That is, the potential risk of the exposure of the core in vivo can be eliminated.

In addition, the elemental mapping TEM image in Fig. 3c confirms that the shell is comprised of Pt, as verified by the selected-area electron diffraction (SAED) patterns in Fig. 3d. The SAED pattern reveals that the Pt coating is polycrystalline, exhibiting four concentric rings; from the innermost to outermost, these correspond to the (111), (200), (220), and (311) crystal planes of Pt, respectively [18].

Fig. 3e shows the X-ray diffraction (XRD) patterns of the PAN and Pt-coated nanofibers. A broad peak in the $2\theta = 20°–30°$ range from the PAN nanofibers indicates the amorphous characteristic of polymeric PAN [21,22]. The red-colored XRD profile, showing discernible peaks at $2\theta = 39.6°$, 46.4°, and 67.1° that correspond to the (111), (200), and (220) planes, respectively, of face-centered cubic (fcc) Pt, confirms that the electroplated nanofibers are completely covered by high-purity Pt (JCPDS Card 04-0802) [23–26].

The XPS spectrum of Pt in Fig. 3f shows one pair of peaks. These two peaks located at the binding energies of 71.0 and 74.2 eV are respectively attributed to the Pt $4f_{7/2}$ and Pt $4f_{5/2}$ orbital levels of metallic Pt. Note that these two main peaks of the Pt 4*f* electrons are originated from Pt(0). Peaks from Pt(IV), which are related to oxygen-containing Pt species such as PtO and PtO_2, are not observed in the XPS spectrum [27,28], thus indicating that the Pt-coated nanofibers are not oxidized in the process of electroplating (cf. Section 2.1).

Although the initial shape of the as-fabricated Pt-coated micro-ropes was akin to a thin and long strand (see Fig. 4a), the high flexibility of the micro-rope allowed it to be bent in any directions, which facilitated various three-dimensional (3D) conformations as commercial coils do (Fig. 4a–c). This is attributed to the fact that not only the core of Pt-coated nanofibers was composed of a soft polymeric material, but also the Pt shell is thin (cf. Figs. 2 and 3). Note that the second maximum twist induced the micro-rope to be highly- and densely-twisted, resulting in a decrease in its diameter from 250 to 150 μm (Fig. 4b). Furthermore, to explore whether the Pt-coated micro-ropes deform due to the prolonged contact with water, the change in morphology before and after soaking in water for 72 h was compared as described in Fig. 4d. No discernible changes in both morphology and diameter were found, which demonstrated that the Pt-coated micro-rope can be sturdy enough even in blood.

3.2. Compatibility of Pt-coated micro-ropes with catheters

In order to explore the compatibility of the fabricated Pt-coated micro-ropes with commercial catheters, we used commercial catheters to insert the Pt-coated micro-ropes into the in vitro experimental model. Chaperon guiding and inner micro-catheters were obtained from Micro Vention (Table 2). Fig. 5a shows the Pt-coated micro-rope inserted in the catheter, where the innermost micro-rope was in the core of the hollow 4F micro-catheter and the corresponding micro catheter was located in the hollow of the 5F guide catheter. Fig. 5b–h depicts snapshots of the micro-rope delivery process using the catheters. Note that each catheter is delivered using a semi-automatic delivery system developed in-house (cf. Fig. 5b), while the micro-ropes are delivered by hand. First, the guide catheter is inserted and located near the bladder (see Fig. 5c and d). Next, the micro-catheter is delivered to the entrance of the bladder through the guide catheter (Fig. 5e and f). Fig. 5g shows the bladder early in the delivery process, where only one Pt-coated micro-rope is inserted ($N = 1$, cf. Section 2.2); Fig. 5h shows the completely filled bladder with multiple micro-ropes ($N = 40$), which confirms that the Pt-coated micro-rope is compatible with commercial catheters. Note that the bladder is completely stuffed at $N = 40$, with no fluid flow occurring through the bladder. Movie

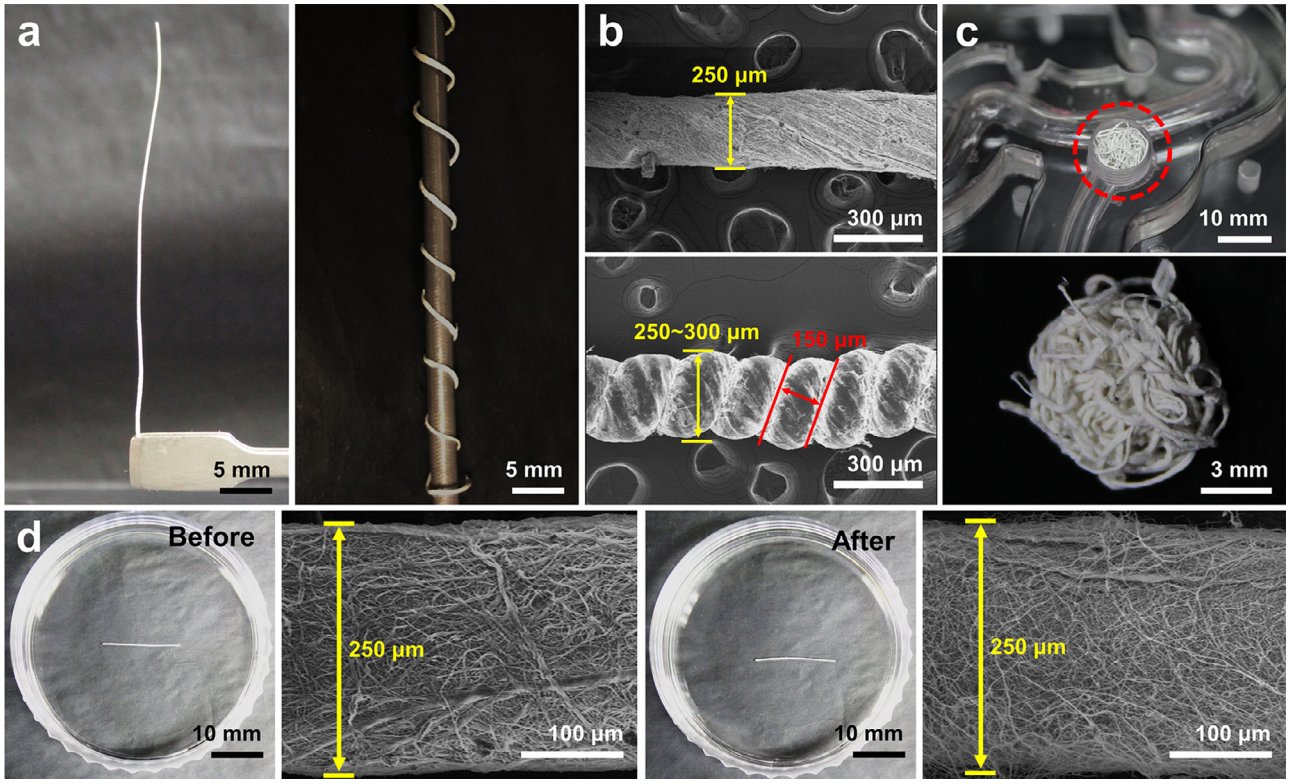

Fig. 4. (a) Photographs of the Pt-coated micro-ropes in straight and helical shapes. (b) SEM images of the Pt-coated micro-rope (top) with and (bottom) without the second maximum twist. (c) Photographs of the highly intertwined Pt-coated micro-ropes at (top) the inside and (bottom) the outside the bladder. (d) Photographs and SEM images of the Pt-coated micro-rope before and after immersing it in water for 72 h.

Table 2
The specification of the commercial catheters used in the experiment.

Catheter type	Parameter	Value
Guide catheter	Size	5F
	Inner diameter [mm]	1.50
	Cather length [cm]	95
	Distal flex. length [cm]	7
Micro-catheter	Size	4F
	Inner diameter [mm]	1.03
	Cather length [cm]	117
	Distal flex. length [cm]	7
	Hydrophilic coating length [cm]	15
	Max. injection pressure [psi]	750
Guide catheter	Size	2.4F
	Inner diameter [mm]	0.79
	Cather length [cm]	100
	Distal flex. length [cm]	11
Micro-catheter	Size	1.7F
	Inner diameter [mm]	0.43
	Cather length [cm]	150
	Distal flex. length [cm]	11
	Hydrophilic coating length [cm]	15
	Max. injection pressure [psi]	750

S1 shows the detailed Pt-coated micro-rope insertion process using the 4F micro and guide catheter.

On the other hand, it should be emphasized that the use of Pt-coated micro-ropes is also feasible through different catheters, as shown in Fig. 6 and Movie S2, in which a micro-rope was inserted in 1.7F micro- and 2.4F guide catheters and its movement inside the catheters was observed. Details of the catheters are described in Table 2. This result clearly demonstrated that the Pt-coated micro-ropes reveal a high compatibility with various kinds of commercial catheters.

3.3. Blocking performance of micro-ropes

Fig. 7a and b shows the PVA fluid (cf. Section 2.2) flowing through the channels and bladder in the in vitro experimental model, exhibiting the difference in flow after the bladder completely stuffed with Pt-coated micro-ropes. Contrary to the case of $N=0$ (Fig. 7a), it is clearly seen that the bladder is completely blocked at $N=40$.

As sketched in Fig. 1e, the upper part of the in vitro experimental model includes the bladder with a length of l and a sub-channel with a length of l_1. Accordingly, the fluid flow through the bladder can be obtained from Darcy's law via Eq. (1), while those through the sub-channel in the upper part and through the lower channel with length of L_2 Fig. 1e) can be described by the Poiseuille equation, as given in Eqs. (2) and (3):

$$Q_1 = \frac{K}{\mu} \cdot \frac{(P_1 - P)}{l} \cdot \pi R^2 \tag{1}$$

$$Q_1 = \frac{\pi R^4}{8\mu} \cdot \frac{(P_1 - P_{atm})}{l_1} \tag{2}$$

$$Q_2 = \frac{\pi R^4}{8\mu} \cdot \frac{(P - P_{atm})}{L_2} \tag{3}$$

where R is the channel radius (cf. Section 2.2), μ is the fluid viscosity (cf. Section 2.2), and P is the pressure at the bifurcation point Fig. 1e). Also, P_1 is the pressure at the exit of the bladder and P_{atm} is the atmospheric pressure at the channel outlets. Note that the pump pressure P_{pump} is the highest applied pressure in the channel before the bifurcation (Fig. 1e), which indicates that $P = P_{pump}$. Also, K is the bladder permeability (Fig. 1e). In addition, Q_1 and Q_2 are the flow rates through outlets 1 and 2 of the model,

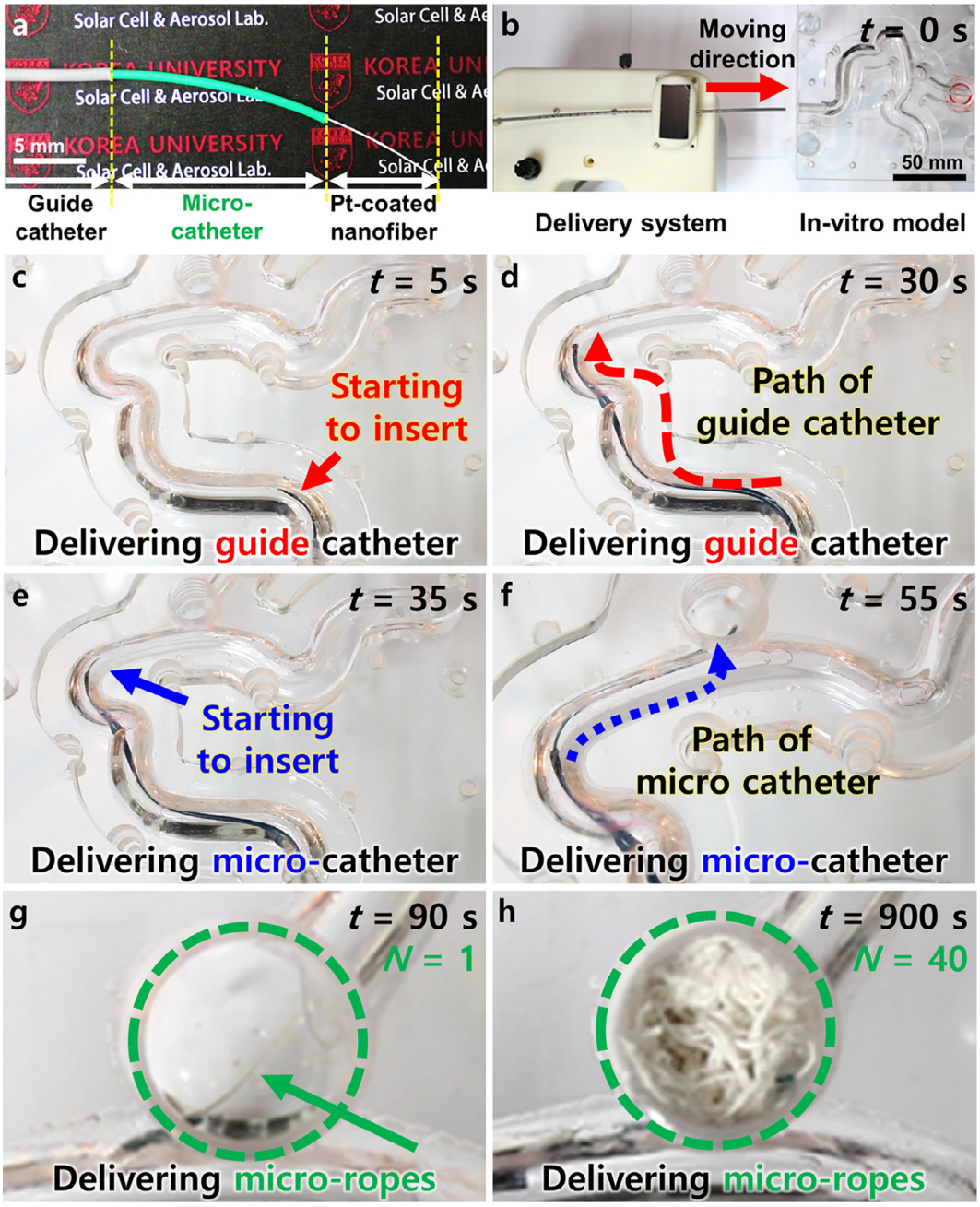

Fig. 5. (a) A photograph of the inserted Pt-coated micro-rope in the catheter, where 4F micro and 5F guide catheters were employed. (b–h) Snapshots in a time sequence for the delivery process of the micro-ropes by (c, d) guide and (e, f) micro-catheter. Magnified photos of the bladder filled with multiple micro-ropes at (g) $N=1$ and (h) $N=40$.

respectively. From Eqs. (1)–(3), the permeability is found as:

$$K = \frac{Q_1 \cdot l}{Q_0 \cdot L_2 + Q_1 \cdot (l - 2L_2)} \cdot \frac{R^2}{8} \tag{4}$$

Note that in the case of $N=0$ (where the bladder is empty, cf. Fig. 7a) the relationship among the flow rates is $Q_1 = Q_2 = Q_0/2$ (where Q_0 is the flow rate through the inlet of the model). This reduces Eq. (4) to $K = R^2/8$. In contrast, when the bladder is completely blocked by the PT micro-ropes ($N=40$, cf. Fig. 7b), fluid flows only through the lower channel (cf. Fig. 7b), corresponding to $Q_2 = Q_0$. Here, because $Q_1 = 0$, also $K=0$ [see Eq. (4)]. Fig. 7c and Table 3 describe the volume of the drained fluid from each outlet as the number of inserted micro-ropes (N) is increased for various diameters of Pt-coated nanofibers. It is seen that the volume of fluid drained from outlet 1 is reduced from 5 to 3.33 to 0 mL as N increased from 0 to 20 to 40, respectively, when using Pt-coated nanofibers with the diameter of 0.50 μm (Fig. 7c and Table 3).

Fig. 7d depicts the variation of the bladder permeability K as the number of Pt-coated micro-ropes N and the corresponding diameter of Pt-coated nanofibers are varied. The value of K without micro-ropes is 0.03125 mm^2 (see red solid line at Fig. 7d); it is gradually decreased from 0.01136 (when the fiber diameter is 0.50 μm), 0.01380 (when the fiber diameter is 0.75 μm), and 0.01518 mm^2 (when the fiber diameter is 1.00 μm) to 0 mm^2 (for all diameters) as the number of micro-ropes N increases from 10 to 40 (Fig. 7d). This indicates that the bladder becomes impermeable

Table 3
Comparison of the volume of drained fluid from outlets 1 and 2 with different numbers of inserted Pt-coated micro-ropes and different diameters of Pt-coated nanofibers.

N	0.50 μm		0.75 μm		1.00 μm	
	Outlet 1 [ml]	Outlet 2 [ml]	Outlet 1 [ml]	Outlet 2 [ml]	Outlet 1 [ml]	Outlet 2 [ml]
0	5.00	5.00	5.00	5.00	5.00	5.00
10	3.87	6.13	4.13	5.87	4.25	5.75
20	3.33	6.67	3.44	6.56	3.75	6.25
30	1.43	8.57	2.45	7.55	2.75	7.25
40	0	10	0	10	0	10

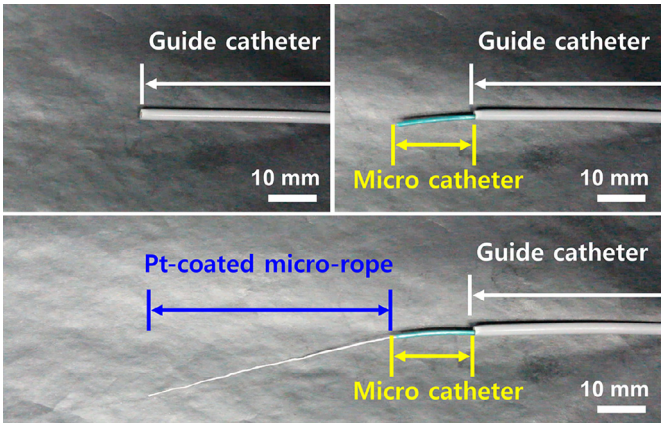

Fig. 6. Photographs of the Pt-coated micro-rope inserted in 1.7F micro and 2.4F guide catheters.

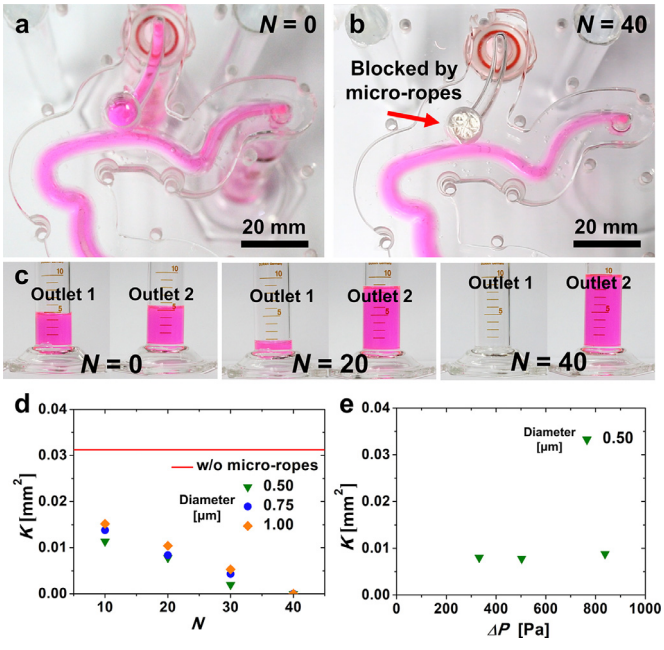

Fig. 7. Photographs of the fluid flows in the in vitro experimental model: (a) without, and (b) with the Pt-coated micro-ropes in the bladder. (c) Comparison of the fluid volumes released from outlets 1 and 2 as a function of the number of inserted micro-ropes in the bladder (*N*). (d) Variation in the permeability *K* with varying number *N* of micro-ropes comprising Pt-coated nanofibers of different diameters. (e) The change of the permeability *K* with varying the pressure of the injected fluid.

when *N* reaches 40 for all nanofiber diameters. The permeability values for different cases (numbers of micro-ropes and fiber diameters) are listed in Table 4.

Table 4
Comparison of the bladder permeability with different number of inserted Pt-coated micro-ropes and different diameters of Pt-coated nanofibers in them. Note that the units of the permeability are 10^{-4} mm^2.

N	Diameter 0.50 μm	0.75 μm	1.00 μm
0	8.33	8.33	8.33
10	4.22	4.87	5.23
20	3.12	3.31	3.94
30	0.89	1.84	2.25
40	0	0	0

The relationship between the pump pressure, P_{pump}, and the total volumetric flow rate, Q_0, is as follows:

$$\Delta P = P_{pump} - P_{atm} = \frac{8\mu}{\pi R^4}(Q_0 \cdot L_1 + Q_2 \cdot L_2) \quad (5)$$

On the other hand, note that the value of *K* increases with an increases in the diameter of the Pt-coated nanofibers Fig. 7d), which means that the thinner Pt-coated nanofibers are more efficient in practice in terms of the permeability reduction, shortening the electroplating time, and reduction in Pt use. On the other hand, accounting for the fact that blood pressure can vary depending on the size and shape of blood vessels, we explored the change in the permeability values with varying fluid pressure. Fig. 7e shows the change of the permeability *K* with varying the pump pressure, ΔP, from Eq. (5). The value of *N* was 20 and the fiber diameter was 0.50 μm. Based on the Poiseuille law [cf. Eqs. (2) and (3)], the flow rate of the injected fluid was adjusted from 0.5 to 2 mL·min^{-1} to change the pressure from one-half of the initial value to the double value. Note that the initial flow rate was 1 mL·min^{-1} (cf. Section 2.2). As a result, the value of *K* varied from 0.00801 to 0.00779 and 0.00881 mm^2, as the pressure varied from one-half of the initial value to the double value, which confirmed that the permeability was almost constant regardless of the change in the fluid pressure.

4. Conclusion

Pt-coated nanofibers can be efficiently and robustly prepared using electrospinning followed by electroplating. Mats of these nanofibers can be tightly twisted to form Pt-coated micro-ropes, which are feasible, effective and attractive for endovascular coil embolization. The developed Pt-coated micro-ropes exhibit reasonable compatibility with commercial delivery catheters, and also reveal high packing performance resulting in negligible permeability as demonstrated in vitro experiments.

Declaration of Competing Interest

The authors have no financial interests to declare.

Acknowledgements

This research was supported by the Technology Development Program to Solve Climate Changes of the National Research Foundation (NRF) funded by the Ministry of Science, ICT & Future Planning (NRF-2016M1A2A2936760), NRF-2017R1A2B4005639, and NRF-2013R1A1A2057994. This study was also supported in part by grants of Korea University (K1807961).

Supplementary materials

Supplementary material associated with this article can be found, in the online version, at doi:10.1016/j.actbio.2019.10.015.

References

[1] D.J. Nieuwkamp, L.E. Setz, A. Algra, F.H. Linn, N.K. de Rooij, G.J. Rinkel, Changes in case fatality of aneurysmal subarachnoid haemorrhage over time, according to age, sex, and region: a meta-analysis, Lancet Neurol. 8 (7) (2009) 635–642.
[2] A.J. Molyneux, R.S. Kerr, L.-M. Yu, M. Clarke, M. Sneade, J.A. Yarnold, P. Sandercock, I.S.A.T.C. Group, International subarachnoid aneurysm trial (ISAT) of neurosurgical clipping versus endovascular coiling in 2143 patients with ruptured intracranial aneurysms: a randomised comparison of effects on survival, dependency, seizures, rebleeding, subgroups, and aneurysm occlusion, Lancet 366 (9488) (2005) 809–817.
[3] A. Molyneux, R. Kerr, I.S.A.T.C. Group, International subarachnoid aneurysm trial (ISAT) of neurosurgical clipping versus endovascular coiling in 2143 patients with ruptured intracranial aneurysms: a randomized trial, J. Stroke Cerebrovasc. Dis. 11 (6) (2002) 304–314.
[4] C.A. Taschner, X. Leclerc, J.-Y. Gauvrit, A. Kerkeni, M. El-Mahdy, J.-P. Lejeune, J.-P. Pruvo, Safety of endovascular treatment of intracranial aneurysms with a new, complex shaped Guglielmi detachable coil, Neuroradiology 49 (9) (2007) 761–766.
[5] A.J. Molyneux, R.S. Kerr, J. Birks, N. Ramzi, J. Yarnold, M. Sneade, J. Rischmiller, I. collaborators, Risk of recurrent subarachnoid haemorrhage, death, or dependence and standardised mortality ratios after clipping or coiling of an intracranial aneurysm in the international subarachnoid aneurysm trial (ISAT): long-term follow-up, Lancet Neurol. 8 (5) (2009) 427–433.
[6] N. Chalouhi, C.D. BoveNzi, V. Thakkar, J. Dressler, P. Jabbour, R.M. Starke, S. Teufack, L.F. Gonzalez, R. Dalyai, A.S. Dumont, Long-term catheter angiography after aneurysm coil therapy: results of 209 patients and predictors of delayed recurrence and retreatment, J. Neurosurg. 121 (5) (2014) 1102–1106.
[7] M.J. Slob, M. Sluzewski, W.J. van Rooij, The relation between packing and reopening in coiled intracranial aneurysms: a prospective study, Neuroradiology 47 (12) (2005) 942–945.
[8] A.J. Molyneux, A. Clarke, M. Sneade, Z. Mehta, S. Coley, D. Roy, D.F. Kallmes, A.J. Fox, Cerecyte coil trial: angiographic outcomes of a prospective randomized trial comparing endovascular coiling of cerebral aneurysms with either cerecyte or bare platinum coils, Stroke 43 (10) (2012) 2544–2550.
[9] C.G. McDougall, S.C. Johnston, A. Gholkar, S. Barnwell, J.V. Suarez, J.M. Romero, J. Chaloupka, A. Bonafe, A.K. Wakhloo, D. Tampieri, Bioactive versus bare platinum coils in the treatment of intracranial aneurysms: the maps (matrix and platinum science) trial, AJNR Am. J. Neuroradiol. 35 (5) (2014) 935–942.
[10] D.F. Kallmes, N.H. Fujiwara, New expandable hydrogel-platinum coil hybrid device for aneurysm embolization, AJNR Am. J. Neuroradiol. 23 (9) (2002) 1580–1588.
[11] C.A. Taschner, R. Chapot, V. Costalat, P. Machi, P. Courthéoux, X. Barreau, J. Berge, L. Pierot, K. Kadziolka, B. Jean, GREAT—a randomized controlled trial comparing hydrosoft/hydroframe and bare platinum coils for endovascular aneurysm treatment: procedural safety and core-lab-assessedangiographic results, Neuroradiology 58 (8) (2016) 777–786.
[12] J.Y. Lee, J.H. Seo, S.J. Lee, Y.J. Son, Y.D. Cho, H.-S. Kang, M.H. Han, Mid-term outcome of intracranial aneurysms treated with Hydrosoft coils compared to historical controls treated with bare platinum coils: a single-center experience, Acta Neurochir. 156 (9) (2014) 1687–1694.
[13] K.R. Abi-Aad, R.J.N. Aoun, R.J. Rahme, J.D. Ward, J. Kniss, M.J. Kwasny, M.G. Sattur, M.E. Welz, B.R. Bendok, New generation hydrogel endovascular aneurysm treatment trial (HEAT): a study protocol for a multicenter randomized controlled trial, Neuroradiology 60 (10) (2018) 1075–1084.
[14] N. Matsubara, S. Miyachi, Y. Nagano, T. Ohshima, O. Hososhima, T. Izumi, A. Tsurumi, T. Wakabayashi, M. Sakaguchi, A. Sano, A novel pressure sensor with an optical system for coil embolization of intracranial aneurysms, J. Neurosurg. 111 (1) (2009) 41–47.
[15] K. Haraguchi, S. Miyachi, N. Matsubara, Y. Nagano, H. Yamada, N. Marui, A. Sano, H. Fujimoto, T. Izumi, T. Yamanouchi, A mechanical coil insertion system for endovascular coil embolization of intracranial aneurysms, Interv. Neuroradiol. 19 (2) (2013) 159–166.
[16] K. Shintai, N. Matsubara, T. Izumi, S. Miyachi, H. Yamada, N. Marui, T. Wakabayashi, Experimental study of coil delivery wire insertion force in intracranial aneurysm embolization: force discrepancy generated inside the microcatheter through that coil delivery wire passes, Nagoya J. Med. Sci. 81 (2) (2019) 217.
[17] M.-W. Kim, S. An, K. Kim, T.-G. Kim, H.S. Jo, D.-H. Park, S.S. Yoon, A.L. Yarin, Packing of metalized polymer nanofibers for aneurysm embolization, Nanoscale 10 (14) (2018) 6589–6601.
[18] S. An, Y.I. Kim, S. Sinha-Ray, M.-W. Kim, H.S. Jo, M.T. Swihart, A.L. Yarin, S.S. Yoon, Facile processes for producing robust, transparent, conductive platinum nanofiber mats, Nanoscale 9 (18) (2017) 6076–6084.
[19] M. Sadeghi, Pectin-based biodegradable hydrogels with potential biomedical applications as drug delivery systems, J. Biomater. Nanobiotechnol. 2 (01) (2011) 36.
[20] R. Samal, P.K. Sahoo, Synthesis of a biodegradable polyacrylonitrile/sodium silicate nanocomposite fire retardant, Indian J. Technol. 17 (2010) 139–144.
[21] W.-S. Kim, B.-S. Lee, D.-H. Kim, H.-C. Kim, W.-R. Yu, S.-H. Hong, SnO_2 nanotubes fabricated using electrospinning and atomic layer deposition and their gas sensing performance, Nanotechnology 21 (24) (2010) 245605.
[22] N. Chatterjee, S. Basu, S. Palit, M.M. Maiti, An XRD characterization of the thermal degradation of polyacrylonitrile, J. Polym. Sci. B Polym. Phys. 33 (12) (1995) 1705–1712.
[23] M.a. Millán, H.c. Zamora, M.A. Rodrigo, J. Lobato, Enhancement of electrode stability using platinum–cobalt nanocrystals on a novel composite SiCTiC support, ACS Appl. Mater. Interfaces 9 (7) (2017) 5927–5936.
[24] M. Shah, Growth of uniform nanoparticles of platinum by an economical approach at relatively low temperature, Sci. Iran. 19 (3) (2012) 964–966.
[25] Y. Yoon, G. Lee, K. Yoo, J.-B. Lee, Fabrication of a microneedle/CNT hierarchical micro/nano surface electrochemical sensor and its in-vitro glucose sensing characterization, Sensors 13 (12) (2013) 16672–16681.
[26] Y. Tan, X. Dai, Y. Li, D. Zhu, Preparation of gold, platinum, palladium and silver nanoparticles by the reduction of their salts with a weak reductant–potassium bitartrate, J. Mater. Chem. 13 (5) (2003) 1069–1075.
[27] B. Yue, Y. Ma, H. Tao, L. Yu, G. Jian, X. Wang, X. Wang, Y. Lu, Z. Hu, CNx nanotubes as catalyst support to immobilize platinum nanoparticles for methanol oxidation, J. Mater. Chem. 18 (15) (2008) 1747–1750.
[28] A. Venezia, D. Duca, M. Floriano, G. Deganello, A. Rossi, XPS study of pumice–supported palladium and platinum catalysts, Surf. Interface Anal. 19 (1–12) (1992) 543–547.